NORSAR

NORSAR Scientific Report No. 1-2005

Semiannual Technical Summary

1 July - 31 December 2004

Frode Ringdal (ed.)

Kjeller, January 2005

6.3 The 7 April 2004 Flisa, Southern Norway earthquake sequence - eight hypocenter determinations and one focal mechanism

6.3.1 Introduction

On 7 April 2004, a moderately felt magnitude 3.5 earthquake occurred close to Flisa, a small settlement in eastern Norway. Geologically, the earthquake was located northeast of the Oslo Graben at the border of the Baltic Shield. This event was observed at numerous seismic stations and arrays in central and northern Europe, in particular the four Fennoscandian IMS arrays (ARCES, FINES, Hagfors, and NORSAR) observed clear P and S onsets. However, most important is that the event occurred in the vicinity of the NORSAR array (closest epicentral distance less than 20 km) and that therefore a precise event location can be achieved. Fig. 6.3.1 shows the geology of the region and a blue circle, indicating the source area of the event.

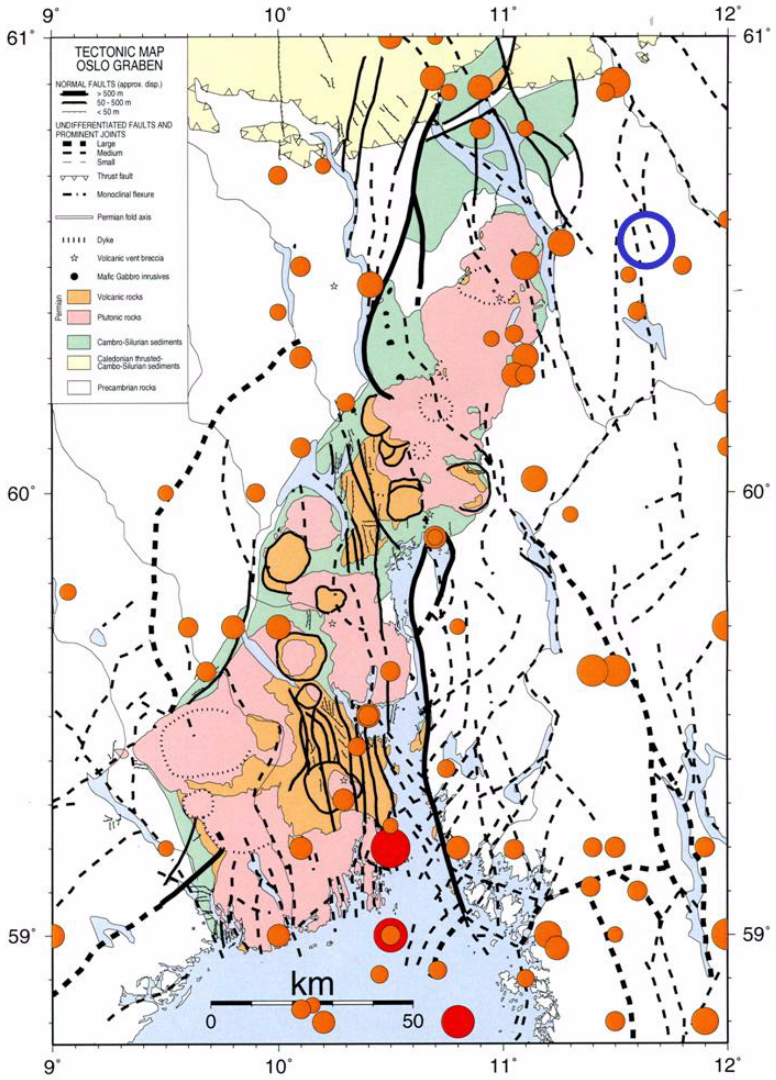

Fig. 6.3.1. Tectonic map of the Oslo Graben area with the source region (blue circle) of the Flisa earthquake sequence (modified from Hicks, 1996). Red symbols show recent seismicity in the region.

Travel-time calibration of the stations of the CTBTO International Monitoring System (IMS) is a major task for CTBT related research at many institutions. For such calibration the availability of recordings from well located seismic events is essential.

A seismic event located so close to an array with 63 single sensors distributed over 42 sites gives a rare opportunity to obtain a very precise location and thereby contribute to the data base of useful ground-truth events. For this event clear P and S onsets were found at all 42 sites of the NORSAR array.

6.3.2 Absolute location of the main shock

Although many observations were available from stations all over Fennoscandia and Central Europe, only the closest stations were used for the event location. The hypocenter determination of the main shock included several steps.

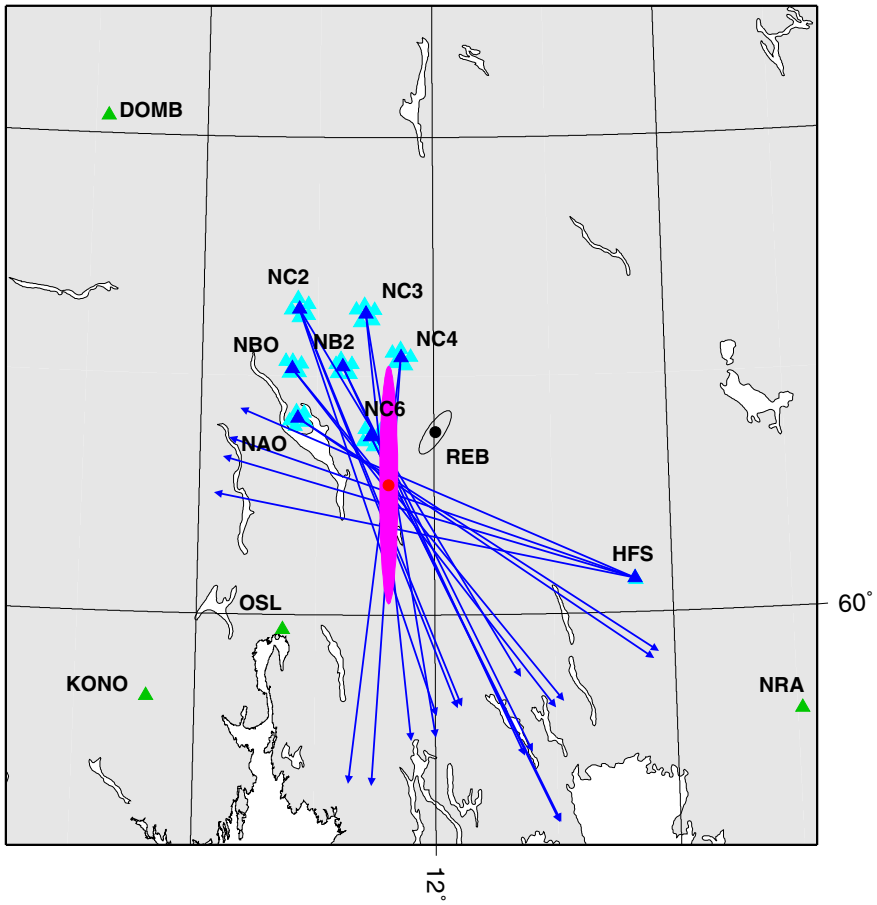

Fig. 6.3.2. The map shows all stations used to locate the main shock. Backazimuth observations at Hagfors and the NORSAR subarrays are shown by blue lines. Also shown are the epicenter (red dot) and the epicentral area (magenta ellipse) as estimated from these observations (99.99% confidence area), and the event location as published in the Reviewed Event Bulletin (REB) of the IDC in Vienna. All single array sites are plotted with blue symbols (the reference sites in dark blue) and all nearby located single sites of the Norwegian and the Swedish national networks are shown in green.

In an initial step, all backazimuth observations of P- and S-type onsets from the NORSAR array and the Hagfors array in Sweden were used to define an initial epicenter. The seven sub-arrays of NORSAR were individually analyzed as small aperture arrays and the backazimuth determined by plane-wave-fit. 158 crossing points could be calculated between the backazimuth observations. Then a common mean crossing point was determined together with its uncertainty. This crossing point defines the starting epicenter for the final inversion. Fig. 6.3.2 shows a map of all backazimuth observations and the calculated epicenter; the uncertainty region is indicated in magenta, which is just the formal error calculated from the single backazimuth uncertainties. This error ellipse does not take in account the actual close geometry between event and observing stations and therefore the error ellipse becomes too elongated in the south-north direction. In addition, the event location as given in the REB by the IDC in Vienna is also shown, which is definitely outside the possible source area already defined by the backazimuth observations.

The second step was the determination of an initial estimate for the final inversion of the hypocenter. Readings at stations with a P and an S onset with the same ray-path geometry, e.g., Pb and Sb or Pn and Sn (assuming a constant v_p/v_s ratio), the v_p/v_s ratio, and the source time are a function of the P-onset time and the travel-time difference between P and S onset (Wadati, 1933). For the Flisa event all observed first P and S onsets at epicentral distances of less than 1° were used for the Wadati-diagram. Fig. 6.3.3 shows the results of this analysis. A mean v_p/v_s ratio of 1.74 was found for all observations and it is easy to see that the source time is determined by the time when the S-P travel-time difference becomes zero. The estimated v_p/v_s ratio is very close to $\sqrt{3}$, which is used in NORSAR's standard velocity model for Fennoscandia (Mykkeltveit & Ringdal, 1981).

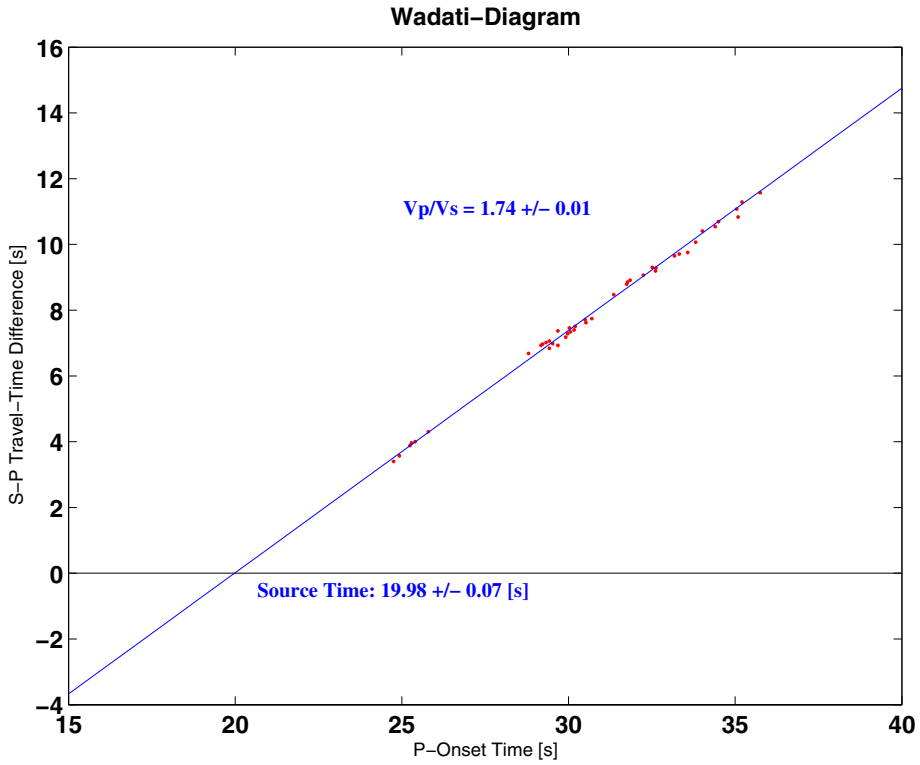

Fig. 6.3.3. The Wadati-diagram for the Flisa main shock defines the mean Vp/Vs ratio and the source time; the given uncertainties correspond to one standard deviation.

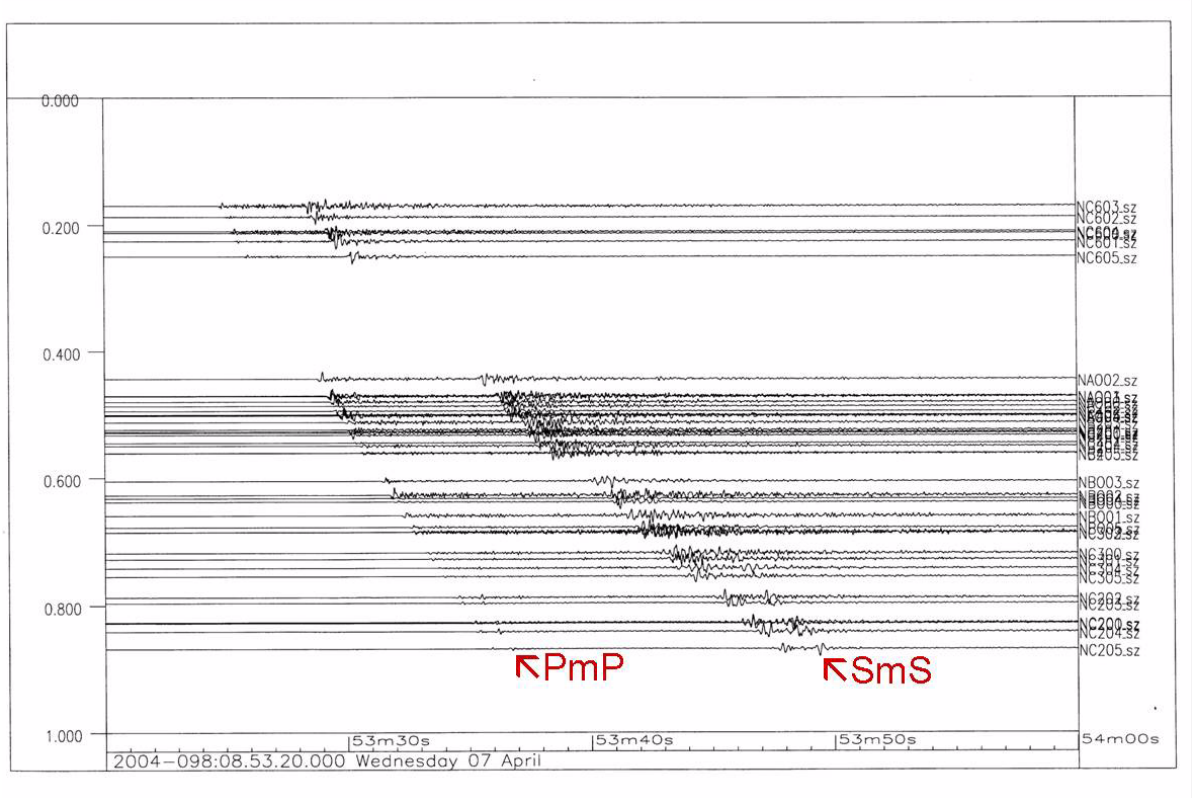

Fig. 6.3.4. Seismogram section of the original vertical traces as recorded at the 42 sites of the NORSAR array. The vertical axes is the distance in degrees from the epicenter. Note the clear PmP and SmS onsets from about 0.8° epicentral distance on. All traces are individually normalized.

As can be seen from Fig. 6.3.4, the Moho-reflections PmP and SmS have clear onsets at all sites of the NORSAR subarray NC2. Such reflections from interfaces below the hypocenter give additional constraints for the event's depth.

In former studies (e.g., Aki et al., 1977; Gundem, 1984; Bischoff et al., 2004) the mean depth to the Moho below the NORSAR array was estimated to be about 35 km. Taking this and the slightly higher v_p/v_s ratio into account, a first, modified velocity model was derived to locate the event (see Table 6.3.1).

Table 6.3.1. The initial velocity model used for locating the Flisa earthquake

Depth (km)	P Velocity (kms^{-1})	S Velocity (kms^{-1})
0.0	6.20	3.569
16.0	6.20	3.569
16.0	6.70	3.857
35.0	6.70	3.857
35.0	8.15	4.705
95.0	8.15	4.705

In the next step, all the initial results were put together and the event was located by applying the location program HYPOSAT (Schweitzer, 2001). For the final inversion not only the array observations but also readings from four nearby seismic stations were used to reduce the azimuthal gap. The results of this inversion are listed as NORSAR_1 in Table 6.3.3.

However, the model uncertainties may still have an effect on the solution. The inversion algorithm used to calculate the hypocenter cannot simultaneously invert for the velocity structure of the region. To find the best model, a systematical trial-and-error process of several steps was performed. During such inversions, the main question is always which possible model types could explain the data equally well and whether the hypocenter determination in such cases will move away to another source area.

The mean P velocities of the model are assumed to be those obtained from former studies (Aki et al., 1977; Mykkeltveit & Ringdal, 1981; Gundem, 1984). The corresponding S velocities are defined by the results of the Wadati-diagram. Therefore, only changes in the mean depth of the Conrad or the Moho discontinuities may influence the locations.

As a first step, the influence of the Moho discontinuity on the location results was tested. Therefore, the hypocenter inversion was repeatedly performed after moving this discontinuity in 1 km steps from 32 to 38 km depth. The result of this test was that the RMS values varied by 20% and the weighted L1 norm of all residuals by 31%. Rejecting all models with more than 10% RMS or weighted L1 norm deviation from the minimum values, the located epicenter varied within +/- 0.14 km of the initial estimate. The effect on the source depth was a bit larger (+/- 0.8 km). The best data fit was achieved with Moho depths at 34 and 35 km.

During the second test the Moho depth was fixed at 35 km and the Conrad discontinuity was varied in 1 km steps between 13 and 26 km depth. Then the RMS values varied by 26.6% and the weighted L1 norm by 25.9%. Rejecting again all results with more than 10% deviation from the smallest RMS or L1 norm value, the source depth varied by +/- 0.4 km and the epicenter by +/- 0.45 km. The smallest RMS and L1 norm values were achieved with depths of the Conrad discontinuity at 20 and 21 km. This is deeper than in the standard Fennoscandia velocity model, which has a border between upper and lower crust at 16 km (Mykkeltveit & Ringdal, 1981; see also Table 6.3.1). However, Bischoff et al. (2004) had already strong indications from their Rayleigh-wave-dispersion curve study for a thicker upper crust below the NORSAR array and they received in their inversion a depth of the Conrad discontinuity at about 20 km. Therefore, in this study the Conrad discontinuity is assumed to be at 20 - 21 km depth.

In the last two steps, the Conrad discontinuity was fixed, once at 20 and once at 21 km, and the Moho depth was again systematically varied between 33 and 37 km. Rejecting all solutions with more than 10% deviation from the smallest RMS or weighted L1 norm values, the final acceptable depth range for the Moho was determined to be 34 - 35 km. For the best solutions the source parameters varied only slightly: the latitude between 60.551˚ and 60.554˚, the longitude between 11.649˚ and 11.653˚, the depth between 22.1 and 23.3 km, and the source time between 08:53:19.834 and 08:53:20.005.

The solution with the absolute smallest RMS was found for a Conrad discontinuity at 21 km depth and a Moho at 35 km depth. The solution with the smallest weighted L1 norm value was found for the combination: Conrad discontinuity at 20 km depth and Moho at 34 km depth. However, since the differences between these solutions are very small and since they all are

inside the 99.99% confidence region, the selection of such details of the final model is not critical. Therefore, the finally chosen model has the Conrad discontinuity at 20 km depth and the Moho discontinuity is located at a depth of 35 km. These two values are also in best agreement with the results of Bischoff et al., 2004 (see Table 6.3.2).

Table 6.3.2. The final mean velocity model used for locating the Flisa earthquake

Depth (km)	P Velocity (kms^{-1})	S Velocity (kms^{-1})
0.0	6.20	3.569
20.0	6.20	3.569
20.0	6.70	3.857
35.0	6.70	3.857
35.0	8.15	4.705
95.0	8.15	4.705

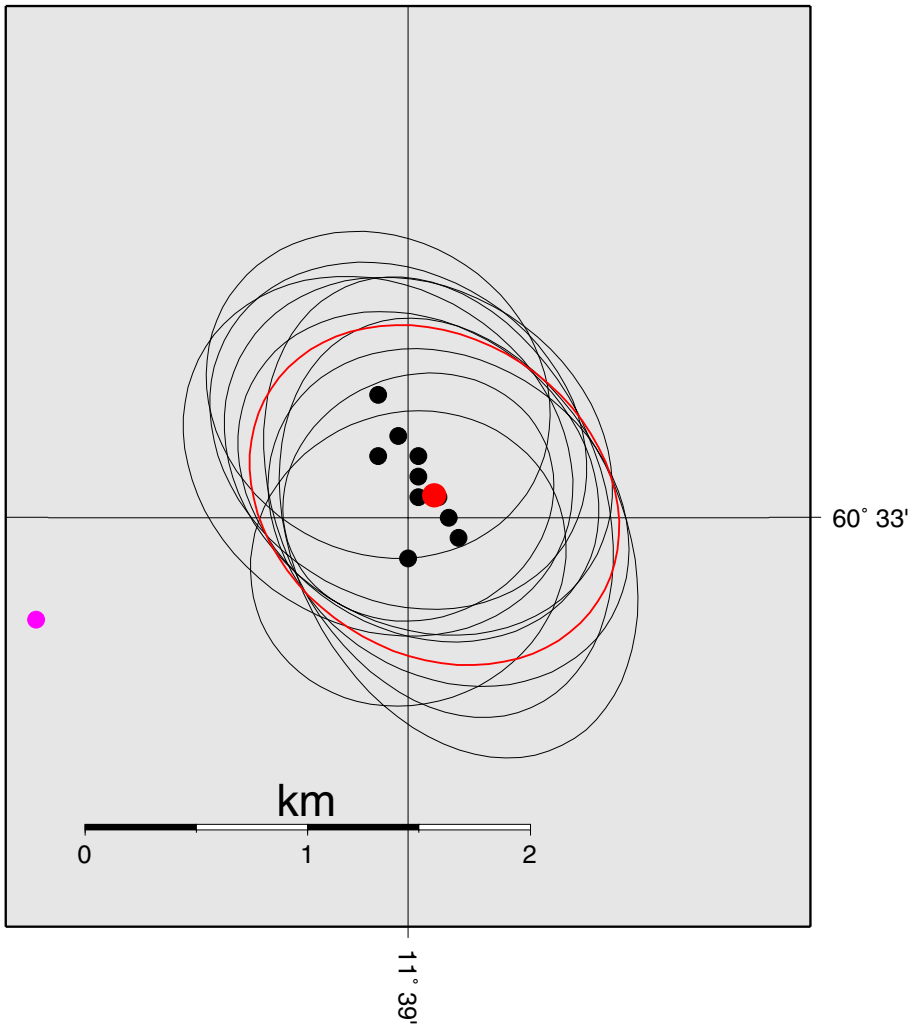

Fig. 6.3.5. Close-up map of locations determined during the model-sensitivity tests. All locations shown in black have RMS and L1 norm values not more than 10% larger than for the final inversion result (red) using the model listed in Table 6.3.2. All error ellipses are for 99.99 confidence level. For comparison the start epicenter from the backazimuth estimates only is also shown (magenta point without error ellipse).

The results of the last inversion are also listed in Table 6.3.3 as solution NORSAR_F. In Fig. 6.3.5 a map with all locations shown including their 99.99% confidence limits (in black), which were found during the model tests and for which the RMS and the weighted L1 norm values are not more than 10% larger than the values for the final inversion. The solution shown in red is the result of the final solution. Note that all solutions calculated for the different models and which have low RMS and weighted L1 norm values lay inside the 99.99 confidence limits of the final solution. The point in magenta shows the epicenter of the start solution, calculated only by the backazimuth observations, and demonstrates the benefits one can achieve from array data.

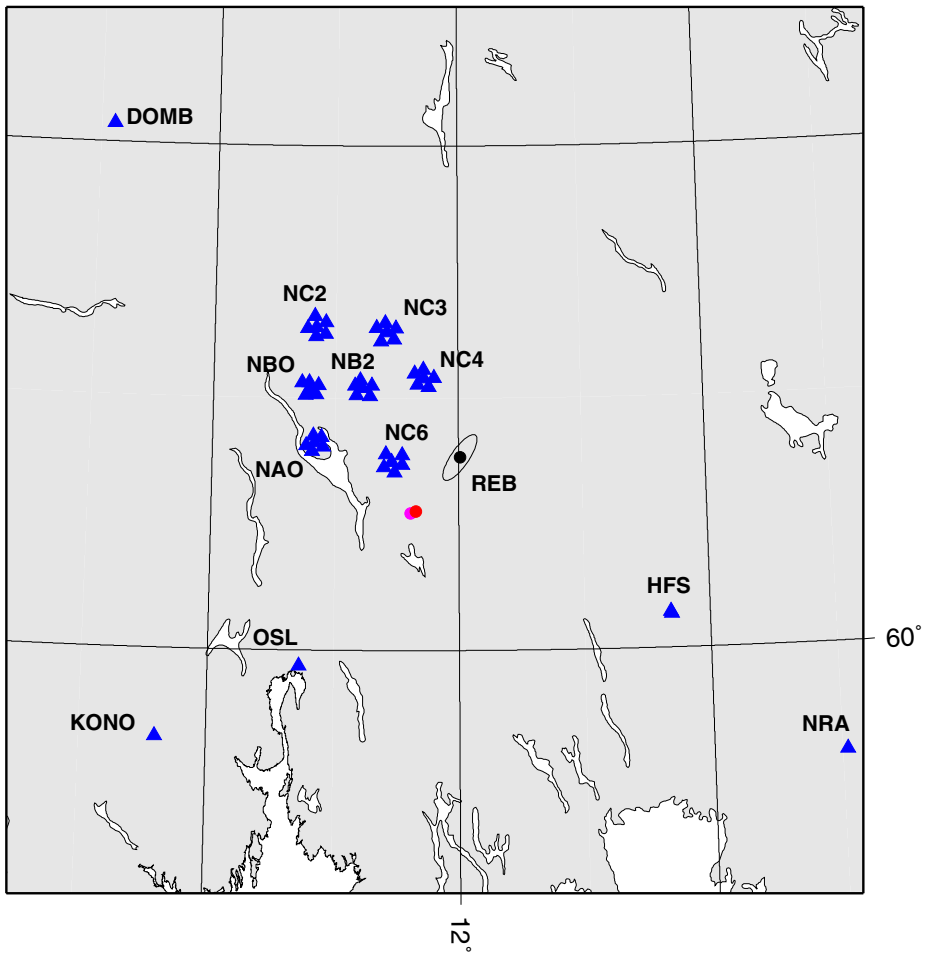

Fig. 6.3.6. The Map shows locations of the Flisa main shock. The red symbol shows the epicenter of the final inversion from this study. The 99.99% confidence ellipse is also plotted but is too small to be seen. In addition we show the epicenter calculated from the backazimuth observations (in magenta), the location results of the IDC, and all stations used in this study to locate the earthquake.

Fig. 6.3.6 shows the results for the final location (NORSAR_F), its 99.99% error ellipse, the stations used, and for comparison the REB location and the epicenter determined only by backazimuth observations (in magenta, now without error ellipse). Note that the error ellipse for the epicenter of the main shock is such small that it is inside of the symbol plotted for the epicenter itself. All numerical values of the location results can be found in Table 6.3.3.

Using the 99.99% (about 3.886 standard deviations in the case of one single parameter) probability limits for the main hypocenter, all the epicenter coordinates are determined within 1 km uncertainty. The model sensitivity tests also showed that the remaining model uncertainties keep the epicenter inside these limits. Therefore, the epicenter of the event can be called a GT-1 event. The uncertainty of the depth determination is slightly larger, in particular due to the influence of the modelling errors. The sensitivity tests showed a bit more than 1 km variation in the depth estimates. Together with the location uncertainty the depth uncertainty is about 2 km. Therefore, this earthquake with a hypocenter in the lower crust can be used to calibrate regional travel-times curves.

Table 6.3.3. Results of the Flisa main shock location. Note that all errors for results of this study are given for 99.99% confidence limits. The IDC uses a 90% confidence limit in its bulletins.

Method	Lat [°]	Lon [°]	Time	Depth [km]	Confidence Limits					Number of Defining Parameters
					Azimuth [°]	Lat / Smaj [km]	Lon/ Smin [km]	Depth [km]	Time [s]	
REB	60.7657	12.0119	08:53:21.18	0.0	35	- 12.0	- 3.9	Fixed	0.73	10
Back-azimuths	60.545	11.613	-	-	-	50.1 -	3.8 -	-	-	158
Wadati	-	-	08:53:19.98	-	-	-	-	-	0.27	43
NORSAR_1	60.5479	11.6501	08:53:20.10	22.7	66.9	0.87/ 0.90	0.84/ 0.87	1.1	0.10	244
NORSAR_F	60.5511	11.6526	08:53:19.96	22.5	123.1	0.74/ 1.06	0.75/ 0.79	0.9	0.09	237

6.3.3 Relative locations for the whole event sequence

In addition to the main shock with its high quality hypocenter determination, one foreshock and seven aftershocks were observed at the NORSAR array and some also at the Hagfors array in Sweden. The foreshock was about 2.5 magnitude units smaller than the main event and was not felt. The aftershocks, which were of even smaller magnitude, were also not felt. Fig. 6.3.7 shows the uncorrected amplitude-power spectra of the main shock, the foreshock and the first aftershock as observed at NC602, one of the seismometer sites closest to the events.

When possible, the onset times of P and S waves were measured by cross-correlation methods. If this was not possible due to a low signal-to-noise (SNR) ratio, the relative onset times were estimated by following common features of the pulse forms from one site to the next. The foreshock and six of the seven known aftershocks could be located relatively to the main shock by applying a master-event algorithm (Schweitzer, 2002). For the foreshock and the first after-

shock recordings from the Hagfors array could also be used. For these two events, a better control of the relative location can be assumed, since the defining data are not exclusively from one direction. Table 6.3.4 gives all details of the estimated relative locations and Fig. 6.3.8 shows a map of all located events. No confidence region is shown for the main shock, since if the main shock is moved all relatively located events will move as a whole group by the same amount. The shown error ellipses for the relatively located events correspond with 99.99% confidence regions.

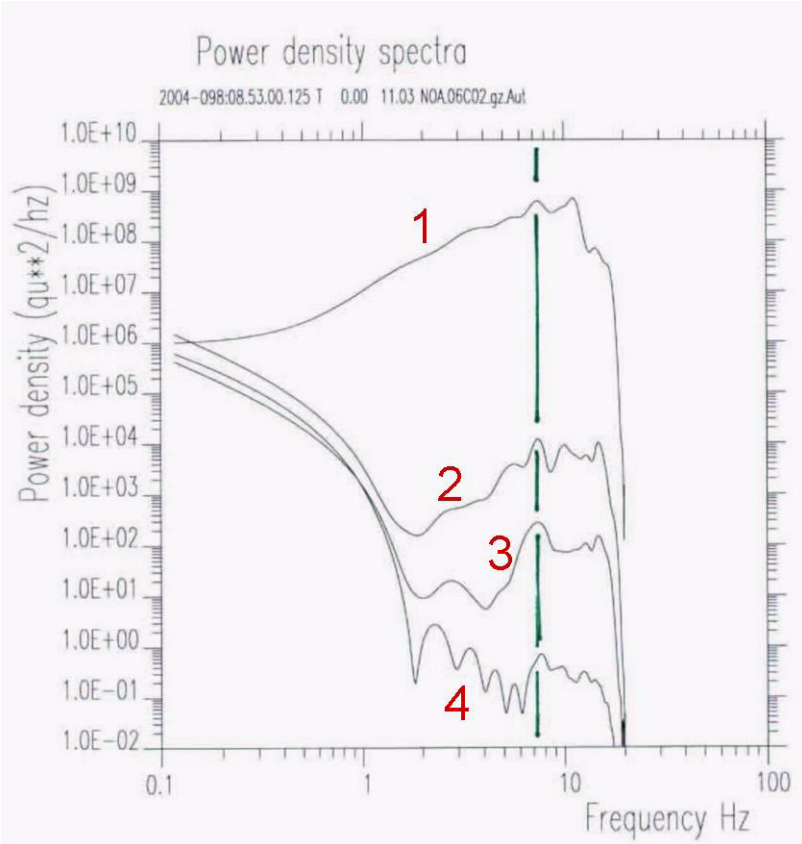

Fig. 6.3.7. Uncorrected power-density spectra of the main shock (1), the foreshock (2), the first aftershock (3), and a noise sample (4) as recorded at the NORSAR array site NC602. The spectral peak for all spectra at about 8 Hz is best explained as a station effect. Note the large range of magnitudes for the different events.

The error ellipse of the foreshock overlaps with the main event, occurring ca. 13 seconds later. This connects these two events closely together to the same rupture plane. Such conclusion cannot be made for the aftershocks, which all occurred in the same source region and depth, but about 1 - 3 km apart from the main shock. For a magnitude 3.5 event the rupture length should not have such an extension. Since all aftershocks are located in the same area, we can either assume that the relative location of these smaller events show some systematic bias or that the first two larger events changed the whole stress field at this place such that the aftershock sequence could occur.

Table 6.3.4. Listing of all relative locations for the whole Flisa earthquake sequence with the main shock as reference event. Given uncertainties for 99.99% confidence limits.

Event	Lat [°]	Lon [°]	N-S [km]	+/- [km]	E-W [km]	+/- [km]	Time [s]	+/- [s]	Depth [km]	+/- [km]
MS	60.5511	11.6526	-	-	-	-	-	-	-	-
FS			-0.214	0.429	-0.099	0.365	-13.43	0.35	-0.001	0.051
AS-1			-1.405	1.784	1.589	1.240	5956.01	1.24	0.353	0.190
AS-2			-1.074	1.853	1.341	0.961	6543.41	1.55	-0.114	0.121
AS-3			-1.945	2.595	1.883	1.171	109659.58	2.14	-0.223	0.190
AS-4			-1.162	0.159	1.407	0.077	112903.46	0.12	-0.038	0.019
AS-5			-1.175	0.618	1.602	0.356	126451.43	0.54	-0.135	0.054
AS-6			-1.536	2.110	1.746	1.188	189400.42	1.79	-0.067	0.194

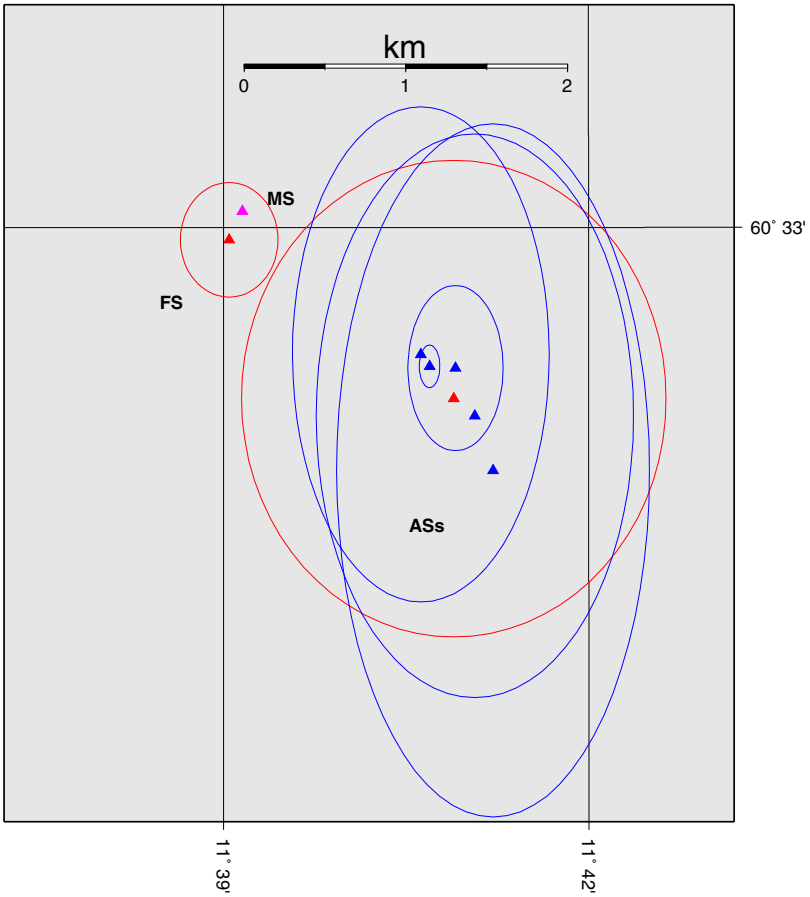

Fig. 6.3.8. A map of all events of the Flisa earthquake sequence as located by a master-event algorithm. The two events shown in red had been relatively located also with Hagfors readings, the magenta triangle show the epicenter of the main shock.

6.3.4 Fault Plane Solution of the Main Shock

As mentioned, the main shock of the Flisa events sequence was observed at almost all stations in Fennoscandia and at many other European stations. Already during the initial analysis of the event it became evident that a polarity change of the first P onsets could be observed for the recordings of the NORSAR array. Fig. 6.3.9 shows first onset recordings from selected NORSAR sites that demonstrate this observation.

After collecting seismograms from all seismic stations up to about 15˚ epicentral distance, a careful analysis of first onset polarities showed that the SNR for all stations from Central Europe was too low for measuring a first onset polarity. However, at almost all stations from Fennoscandia and one in Estonia such a measurement was possible and a classical fault-plane solution could be achieved.

This solution was even better constrained by adding observed polarities from PmP observations at the vertical components of the NORSAR subarray NC2. Fig. 6.3.10 shows a map with the fault-plane solution and the stations from which polarity data were used to derive this solution.

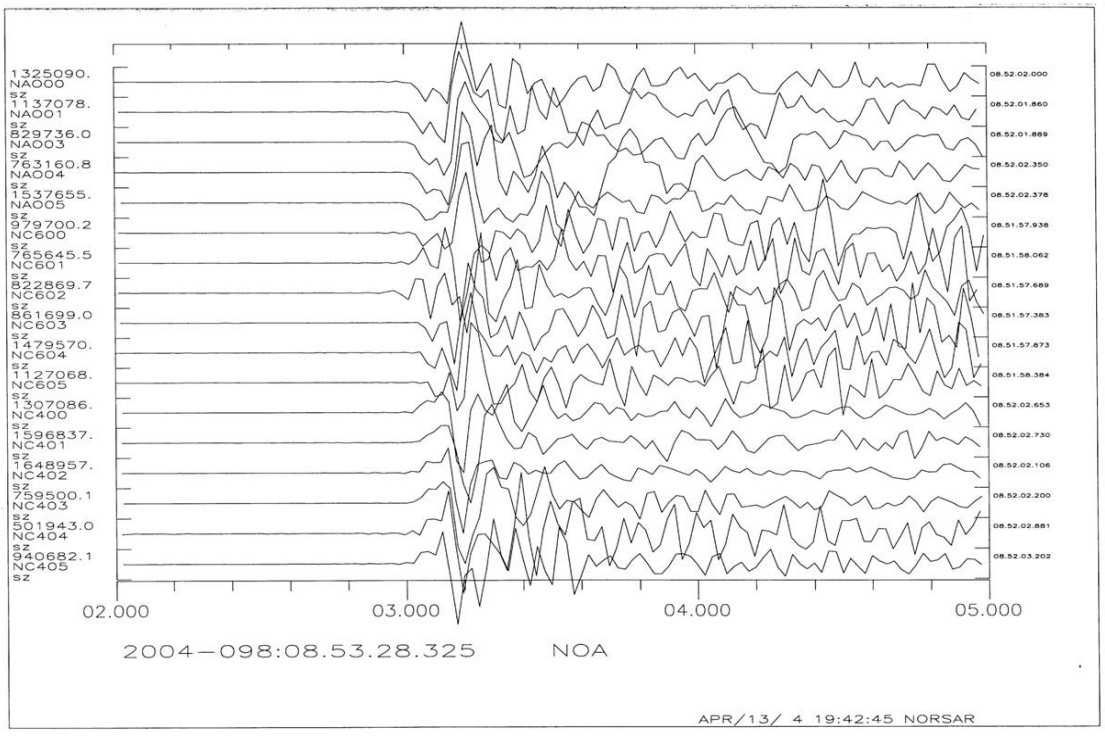

Fig. 6.3.9. P onsets of the Flisa main shock as observed at the NORSAR subarrays NA0, NC4, and NC6. All data are unprocessed but aligned along the first onsets. Note the polarity change from top to bottom.

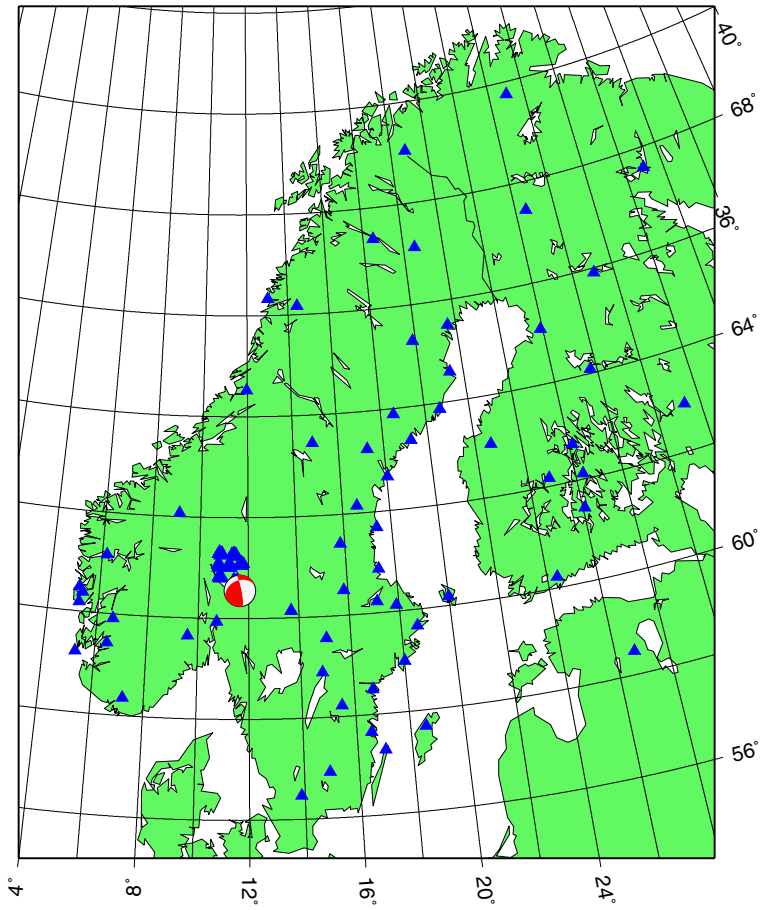

Fig. 6.3.10. The map shows all stations used for determination of the fault plane solution of the Flisa main shock.

The FOCMEC inversion routine (Snoke, 2003) was applied to calculate all possible fault planes, which are in agreement with the observed polarities. The assumption for this type of inversion is that a single double couple can describe the source mechanism. Fig. 6.3.11 shows all observed polarities and the results from FOCMEC. The triangles represent negative and the circles positive first onset polarities.

As fault plane the very steep, north-south striking plane can be assumed since the second plane is horizontally oriented and such a horizontal movement in the lower crust is difficult to achieve. Many earthquakes in and around the Oslo Graben area show similar north-south striking fault planes but a large variability in the orientation of auxiliary plane; almost every type of source mechanism can be observed: normal faulting, strike-slip movements, and reverse faulting (see e.g., Hicks et al., 2000; Lindholm et al., 2000). Although the tectonic features in the lower crust must not the same as at the surface, the geological observations at the surface further support this interpretation as the many mapped faults show a north-south striking direction (see Fig. 6.3.1).

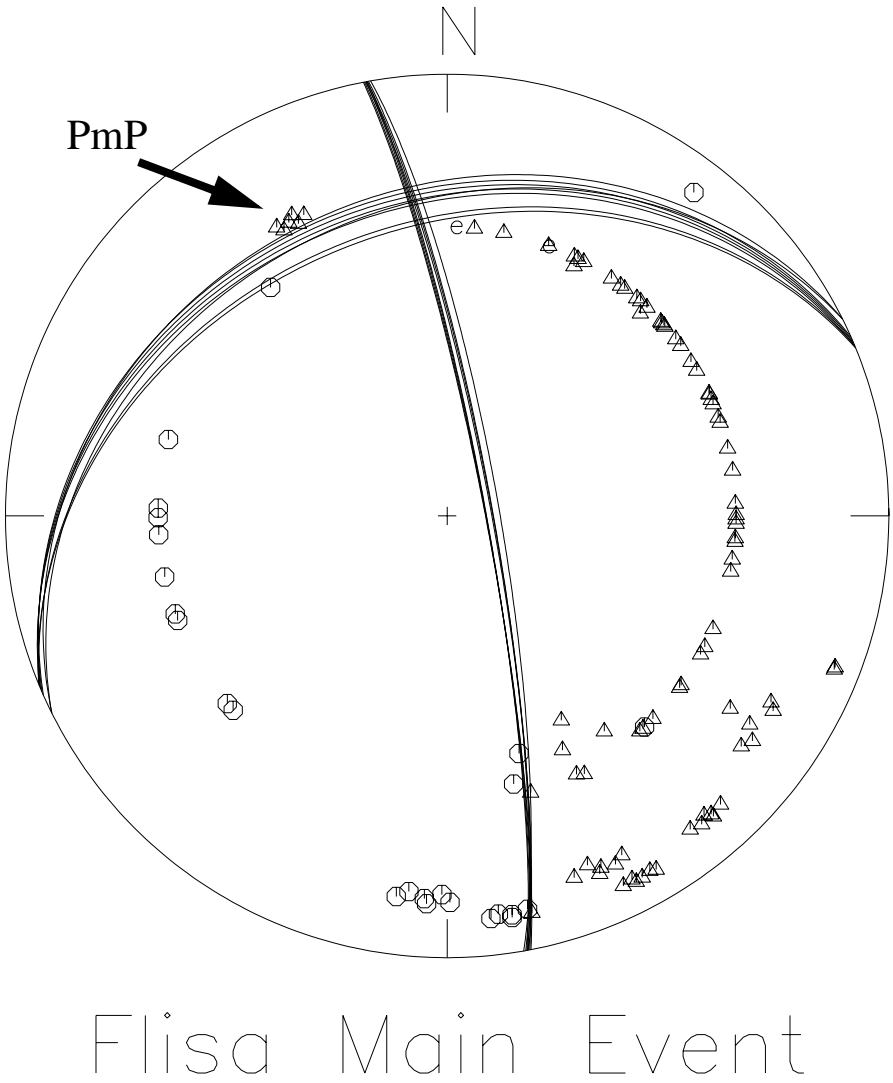

Fig. 6.3.11. Fault-plane solution for the Flisa main shock as derived from first onset polarities. The plot shows all polarities projected on the lower hemisphere. Triangles are negative and circles are positive first onsets. All possible solutions found by FOCMEC (Snoke, 2003) are plotted. The most presumable rupture plane is one of the steep north-south striking fault-planes. Note, the negative polarities of PmP observed at the sites of the NORSAR subarray NC2, which restrict the number of possible solutions.

6.3.5 Conclusions

To calculate a start solution for the hypocenter inversion of the 7 April 2004 Flisa main event, classical location procedures were applied including backazimuth observations, Wadati diagram and an optimized velocity model.

The inversions were performed with the HYPOSAT location program, which can use all available data (onset times of first and later onsets, backazimuth and slowness observations, travel time differences between phases, and different types of corrections) to achieve the best least-squares-fit type solution.

Investigation of model uncertainties associated with changes made to NORSAR's standard velocity model, revealed that the best fit was achieved when the thickness of the upper crust was increased to 20 km. This is also in agreement with recent results of a surface wave study (Bischoff et al., 2004).

Our best location estimate of the Flisa main event is:

Lat:	60.5511˚
Lon:	11.6526˚
Depth:	22.5 km
T0:	08:53:20.0

One foreshock and several aftershocks were observed. After applying the master-event technique, the foreshock and six of the aftershocks could be located relatively to the main event.

The fault-plane solution for the main shock was determined in the traditionally way from first onset observations at numerous stations. In addition, some PmP polarities were used to restrict the solution space. The resulting fault-plane solution shows a north-south striking reverse fault plane, which was presumable also the rupture plane of the main shock.

Acknowledgements

For this study we received data from the University of Bergen for the Norwegian network, from the University in Uppsala for the Swedish network, from the University of Helsinki for the Finnish network, and from ORFEUS the data for all stations contributing to the Virtual European Broadband Seismograph Network (VEBSN). The precise event location and in particular the well defined fault-plane solution would not have been possible without such data exchange, which is gratefully acknowledged.

Johannes Schweitzer

References

Aki, K., A. Christofferson & E. Husebye, E.S. (1977). Determination of the three-dimensional seismic structure of the lithosphere. *J. Geophys. Res.*, **82**, 277-296.

Bischoff, M., J. Schweitzer & T. Meier (2004). Comparison of the Love-Rayleigh discrepancy in central Europe (GRSN) and southern Scandinavia (NORSAR). *NORSAR Sci. Rep.,* **2-2004**, 70-78.

Gundem, M.B. (1984). *2-D seismic synthesis of the Oslo graben*. Cand. Scient. Thesis, University of Oslo, Norway, 164 pp.

Hicks, E. C. (1996). *Crustal stresses in Norway and surrounding areas as derived from earthquake focal mechanism solutions and in-situ stress measurements.* Cand. Scient. Thesis, University of Oslo, Norway, 164 pp.

Hicks, E.C., H. Bungum & C.D. Lindholm (2000). Stress inversion of earthquake focal mechanism solutions form onshore and offshore Norway. *Norsk Geologisk Tidsskrift,* **80**,235-250.

Lindholm, C.D., H. Bungum, E. Hicks & M. Villagran (2000). Crustal stress and tectonics in Norwegian regions determined from earthquake focal mechanisms. In: Nottvedt et al. (eds). Dynamics of the Norwegian Margin. Geological Society London, 167, 429-439.

Mykkeltveit, S., & Ringdal, F. (1981). Phase identification and event location at regional distance using small aperture array data. In: Husebye, E.S. & Mykkeltveit, S. (eds). *Identification of seismic sources – earthquake or underground explosions*, D. Reidel, 467-481.

Schweitzer, J. (2001). HYPOSAT – an enhanced routine to locate seismic events. *Pure appl. geophys.,* **158**, 277-289.

Schweitzer, J.(2002). Some results derived from the seismic signals of the accident of the Russian submarine Kursk. *NORSAR Sci. Rep.*, **1-2002**, 115-121.

Snoke, J. A. (2003). FOCMEC: FOcal MEChanism determinations. In: Lee, W. H. K., H. Kanamori, P. C. Jennings & C. Kisslinger (eds). *International Handbook of Earthquake and Engineering Seismology.* Academic Press, San Diego, Chapter 85.12.

Wadati, K. (1933). On the travel time of earthquake waves. Part. II. Geophys. Mag. (Tokyo) **7**, 101-111.